Nanoparticles size estimation through Mie resonances

Neven Gentil

April 2022

1 Theory

1.1 Vector Spherical Harmonics

First at all, let's describe the general composition of our problem: given an arbitrary particle droped in a certain medium, we hit it with a monochromatic light. With a fixed size and other specifics parameters for electromagnetic materials like the permeability μ or the complex refractive index N, our objective is to, theoretically, compute the electromagnetic field for the medium surrounding the particle and inside this particle itself, in order to find the expression of the scattered light.

Let's start with an arbitrary electromagnetic field represented by the couple of *monochromatic* vector field $(\mathbf{E}, \mathbf{H})$ which satisfies the Maxwell equations:

$$\nabla \cdot \mathbf{E} = 0 \tag{1.1}$$
$$\nabla \cdot \mathbf{H} = 0 \tag{1.2}$$
$$\nabla \times \mathbf{E} = i\omega\mu\mathbf{H} \tag{1.3}$$
$$\nabla \times \mathbf{H} = -i\omega\epsilon\mathbf{E} \tag{1.4}$$

Given the relation $k^2 = \omega^2\epsilon\mu$ and the following formula:

$$\nabla \times (\nabla \times \mathbf{A}) = \nabla(\nabla \cdot \mathbf{A}) - \nabla \cdot (\nabla\mathbf{A}) \tag{1.5}$$

we obtain a couple of *vector wave equation*:

$$\nabla^2\mathbf{E} + k^2\mathbf{E} = 0 \tag{1.6}$$
$$\nabla^2\mathbf{H} + k^2\mathbf{H} = 0 \tag{1.7}$$

where ∇^2 is the vector Laplace operator, that is to say, we explicitly have $\Delta\mathbf{A} = \nabla^2\mathbf{A} = (\nabla \cdot \nabla)\mathbf{A}$.

An important thing to notice is that any vector field with zero divergence and satisfying the vector wave equation is a valid electric/magnetic field where we can obtain the corresponding magnetic/electric field by the curl (1.3)/(1.4).

In this way, it is possible to create a vector function $\mathbf{M}$ depending on a scalar function ψ and an arbitrary constant vector $\mathbf{c}$:

$$\mathbf{M} = \nabla \times (\mathbf{c}\psi) \tag{1.8}$$

where $\mathbf{M}$ directly satisfies the condition $\nabla \cdot \mathbf{M} = 0$. If we replace the expression of $\mathbf{M}$ in the vector wave equation, and thanks to (1.5), we easily obtain:

$$\nabla^2\mathbf{M} + k^2\mathbf{M} = \nabla \times [\mathbf{c}(\nabla^2\psi + k^2\psi)] \tag{1.9}$$

To satisfy the vector wave equation, ψ should also satisfy the equivalent scalar wave equation:

$$\nabla^2\psi + k^2\psi = 0 \tag{1.10}$$

where, this time, ∇^2 is the scalar Laplace operator. By the way, as described above, if we denote $\nabla \times \mathbf{N} = k\mathbf{M}$, we have the perpendicular vector field of the associated artificial one, also satisfying the vector wave equation. Finally, we created the vector harmonics $\mathbf{M}$ and $\mathbf{N}$ with the scalar generating function ψ associated to our initial electromagnetic field.

1.2 Associated Factors

The main idea to compute all solutions required is the following: given an incident electromagnetic field, we use the boundary conditions on the surface of our particle to get all fields resulting from interaction. Thereby, it could be interesting to use the spherical polar coordinates during the calculation and particularly to express the boundary conditions. That is why we have constructed the vector harmonics above. Indeed, if we replace the constant vector $\mathbf{c}$ by the radial coordinate $\mathbf{r}$, $\mathbf{M}$ is always a solution of the vector wave equation but, this time, for the spherical polar coordinates linked to the particle. In this way, from (1.10), we obtain:

$$\begin{aligned} \frac{1}{r^2}\frac{\partial}{\partial r}(r^2\frac{\partial\psi}{\partial r}) \quad &+ \\ \frac{1}{r^2 sin(\theta)}\frac{\partial}{\partial\theta}(sin(\theta)\frac{\partial\psi}{\partial\theta}) \quad &+ \\ \frac{1}{r^2 sin(\theta)}\frac{\partial^2\psi}{\partial^2\phi} \quad &+ \\ k^2\psi \quad &= 0 \end{aligned} \tag{1.11}$$

Obviously, from the previous formula, we can separate each variable to create ψ:

$$\psi(r, \theta, \phi) = R(r)\Theta(\theta)\Phi(\phi) \tag{1.12}$$

Thereby, when substitued (1.12) into (1.11), we obtain three different equations, depending respectively on r, θ and ϕ which might be solved separately.

Finally, this kind of generating function ψ satisfying the scalar wave equation (1.10) is expressed in two *even* (ψ_e) and *odd* (ψ_o) functions as follow:

$$\psi_{emn} = cos(m\phi)P_n^m(cos\theta)z_n(kr) \tag{1.13}$$
$$\psi_{omn} = sin(m\phi)P_n^m(cos\theta)z_n(kr) \tag{1.14}$$

where the parity of our original function is led by the *cosinus* and *sinus* attached with the ϕ variable and the *angle-dependent* m variable.

The other angular part described by θ , as a *Legendre's differential equation*, is solved by the *associated Legendre functions* of the first kind $P_n^m(cos\theta)$ orthogonally defined on the n variable.

Moreover, the radial part, described by r, might be reintroduced as follow:

$$\rho\frac{d}{d\rho}(\rho\frac{dZ}{d\rho}) + [\rho^2 - (n + \frac{1}{2})^2]Z = 0 \tag{1.15}$$

where we assume that $\rho = kr$ and $Z = R\sqrt{\rho}$. Thereby, to solve the previous equation, we can use any linear combination of the spherical Bessel functions j_n, y_n, $h_n^{(1)} = j_n + iy_n$ or $h_n^{(2)} = j_n - iy_n$: we named this kind of combination z_n.

Note that m and n are produced by subsidiary conditions when obtaining these three equations by rewriting (1.11) with separate variables: it is inherent to our physical assumptions.

In the end, we can retrieve our initial vector spherical harmonics generated by ψ_{emn} or ψ_{omn}:

$$\mathbf{M}_{emn} = \nabla \times (\mathbf{r}\psi_{emn}) \tag{1.16}$$
$$\mathbf{M}_{omn} = \nabla \times (\mathbf{r}\psi_{omn}) \tag{1.17}$$
$$\mathbf{N}_{emn} = \frac{\nabla \times \mathbf{M}_{emn}}{k} \tag{1.18}$$
$$\mathbf{N}_{omn} = \frac{\nabla \times \mathbf{M}_{omn}}{k} \tag{1.19}$$

At this point of the theory, it is still possible to restrain our hypothesis and more precisely the shape of the incident light. Let's consider a planar incident electromagnetic wave E_i. Now, we can easily describe this wave in terms of vector spherical harmonics:

$$\begin{aligned}\mathbf{E}_i = \sum_{m=0}^{\infty}\sum_{n=m}^{\infty} & B_{emn}\mathbf{M}_{emn} + B_{omn}\mathbf{M}_{omn} \\ & + A_{emn}\mathbf{N}_{emn} + A_{omn}\mathbf{N}_{omn}\end{aligned} \tag{1.20}$$

where B_X and A_X are arbitrary factors. Thanks to the orthogonality of all the vector spherical harmonics which could be demonstrated through properties from $cos(m\phi)$, $sin(m\phi)$ and $P_n^m(cos\theta)$, we easily exctract each factor of this linear summation (1.20):

$$\mathbf{B}_{emn} = \frac{\int_0^{2\pi}\int_0^{\pi} \mathbf{E}_i \cdot \mathbf{M}_{emn} sin\theta d\theta d\phi}{\int_0^{2\pi}\int_0^{\pi} |\mathbf{M}_{emn}|^2 sin\theta d\theta d\phi} \tag{1.21}$$

with here, for instance, the first coefficient. With the orthogonality of the sine and cosine and (1.21), we can also demonstrate that B_{emn} and A_{omn} vanishe for all m and n. Then, for the same reason, B_{omn} and A_{emn} are nonzero only for $m = 1$. Moreover, regarding their behavior and our physical assumptions, we can select the spherical Bessel function replacing z_n: we choose j_n for its finite values close to $r = 0$ and denote it as $^{(1)}$ for the associated vector spherical harmonics. Finally, we obtain:

$$\mathbf{E}_i = \sum_{n=1}^{\infty} B_{o1n}\mathbf{M}_{o1n}^{(1)} + A_{e1n}\mathbf{N}_{e1n}^{(1)} \tag{1.22}$$

Afterward, thanks to a bunch of properties from the associated Legendre functions, we deduce explicitly these two remaining factors B_{o1n} and A_{e1n} from (1.21) or the equivalent expression:

$$\mathbf{E}_i = E_0 \sum_{n=1}^{\infty} i^n \frac{2n+1}{n(n+1)}(\mathbf{M}_{o1n}^{(1)} - i\mathbf{N}_{e1n}^{(1)}) \tag{1.23}$$

Obviously, it is possible to calculate the perpendicular magnetic field H_i with the curl (1.3).

1.3 Boundary Conditions

At this point, we have enough equation relative to the incident plane wave to apply the following boundary conditions:

$$(\mathbf{E}_i + \mathbf{E}_s - \mathbf{E}_I) \times \overrightarrow{e_r} = 0 \tag{1.24}$$
$$(\mathbf{H}_i + \mathbf{H}_s - \mathbf{H}_I) \times \overrightarrow{e_r} = 0 \tag{1.25}$$

where $(\mathbf{E}_s, \mathbf{H}_s)$ and $(\mathbf{E}_I, \mathbf{H}_I)$ are respectively the scattering and internal electromagnetic field resulting from the interaction between the incident field and our particle. Then, we assume that these last fields have the same mathematical shape, when developped in vector spherical harmonics, than $(\mathbf{E}_i, \mathbf{H}_i)$; that is to say, the scattering and internal field are linearly dependent from the incident field up to some factors taking into account the behavior of j_n at the boundary of our particle:

$$\mathbf{E}_I = \sum_{n=1}^{\infty} E_n(c_n\mathbf{M}_{o1n}^{(1)} - id_n\mathbf{N}_{e1n}^{(1)}) \tag{1.26}$$
$$\mathbf{H}_I = \frac{-k_I}{\omega\mu_I}\sum_{n=1}^{\infty} E_n(d_n\mathbf{M}_{e1n}^{(1)} + ic_n\mathbf{N}_{o1n}^{(1)}) \tag{1.27}$$
$$\mathbf{E}_s = \sum_{n=1}^{\infty} E_n(ia_n\mathbf{N}_{e1n}^{(3)} - b_n\mathbf{M}_{o1n}^{(3)}) \tag{1.28}$$
$$\mathbf{H}_s = \frac{k}{\omega\mu}\sum_{n=1}^{\infty} E_n(ib_n\mathbf{N}_{o1n}^{(3)} + a_n\mathbf{M}_{e1n}^{(3)}) \tag{1.29}$$

Note that $^{(3)}$ means we use the spherical Bessel function of the third kind $h_n^{(1)}$ and $\mathbf{H}_X$ has the same factors than $\mathbf{E}_X$ due to the curl (1.3). Moreover, k_I and μ_I are respectively the wave vector and the permeability of the particle.

Now, we can rewrite the boundary conditions on the surface of our imaginary particle from (1.24) with each component separated, that is to say at $r = a$ if we denote by a its radius:

$$\begin{aligned} E_{i\theta} + E_{s\theta} &= E_{I\theta} \\ E_{i\phi} + E_{s\phi} &= E_{I\phi} \\ H_{i\theta} + H_{s\theta} &= H_{I\theta} \\ H_{i\phi} + H_{s\phi} &= H_{I\phi} \end{aligned} \tag{1.30}$$

where E_{iX}, for instance, denotes the X-component of $\mathbf{E}_i$. Then, we apply the explicit expressions for the incident, scattering and internal field on these previous boundary conditions (1.30) with, needless to say, the detailled expressions of the vector spherical harmonics $\mathbf{M}_X$ and $\mathbf{N}_X$. In this way, we obtain four linear equations revealing the four coefficients arbitrary pushed into $(\mathbf{E}_I, \mathbf{H}_I)$ and $(\mathbf{E}_s, \mathbf{H}_s)$:

$$\begin{aligned} j_n(mx)c_n + h_n^{(1))}(x)b_n &= j_n(x) \\ \mu[mxj_n(mx)]'c_n + \mu_I[xh_n(x)]'b_n &= \mu_I[xj_n(x)]' \\ \mu m j_n(mx)d_n + \mu_I h_n^{(1))}(x)a_n &= \mu_I j_n(x) \\ [mxj_n(mx)]'d_n + m[xh_n^{(1))}(x)]'a_n &= m[xj_n(x)]' \end{aligned} \tag{1.31}$$

where the prime sign means derivation along the same argument between parenthesis. Moreover, we have the following definitions:

$$x = ka = \frac{2\pi Na}{\lambda} \qquad m = \frac{N_I}{N} \tag{1.32}$$

where N_I indicates the refractive index of the particle. In the same way, N is owned by the medium. By the way, it could be intersting to notice that we also have $\rho(a) = x$.

Then, thanks to a basic Gaussian elimination, we can exctract each coefficient. Surprisingly, with some approximation on the spherical Bessel functions depending on the frequency, it is possible to admit the equality between a_n and d_n then b_n and c_n. Furthermore, these two factors could be simplified by introducing the *Riccati-Bessel* functions:

$$\psi_n(\rho) = \rho j_n(\rho) \qquad \xi_n(\rho) = \rho h_n^{(1)}(\rho) \tag{1.33}$$

and we finally obtain the following expressions for the two first coefficients:

$$\begin{aligned} a_n &= \frac{m\psi_n(mx)\psi_n^{'}(x) - \psi_n(x)\psi_n^{'}(mx)}{m\psi_n(mx)\xi_n^{'}(x) - \xi_n(x)\psi_n^{'}(mx)} \\ b_n &= \frac{\psi_n(mx)\psi_n^{'}(x) - m\psi_n(x)\psi_n^{'}(mx)}{\psi_n(mx)\xi_n^{'}(x) - m\xi_n(x)\psi_n^{'}(mx)} \end{aligned} \tag{1.34}$$

1.4 Cross Sections

From now on, we have enough theory to think about the experimental approach and fit all our requirements. That is to say, let's describe the coordinate system through an explicit diagram: As we can see, this reference frame

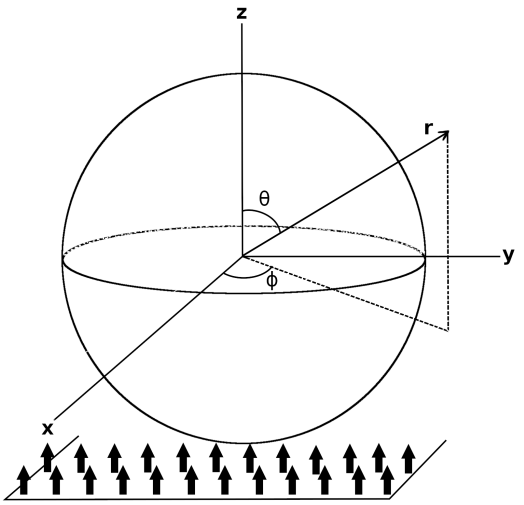

Figure 1: Coordinate System

is really common and our incomming plane wave is going through our particle along the z-axis. That said, our actual way to mesure the particle's size is to, roughly, retrieve the power emitted by it thanks to an optical microscope. Thereby, our goal is currently is to calculate this associated power, that is to say the net rate at which electromagnetic field crosses the surface A of an arbitrary sphere, which might be expressed as follow:

$$W = \int_A \mathbf{S} \cdot \overrightarrow{e_r} dA \tag{1.35}$$

where $\mathbf{S}$ is the *Pointing vector* defined as:

$$\mathbf{S} = \frac{1}{2} Re\left\{\mathbf{E}^* \times \mathbf{H}\right\} \tag{1.36}$$

Note that an arbitrary sign can be added to (1.35) in fonction of our physical assumptions. In this way, we can now compute this power for the scattered electromagnetic field $(\mathbf{E}_s, \mathbf{B}_s)$ and we obtain:

$$W_s = \frac{1}{2} Re\left\{\int_{\phi=0}^{2\pi}\int_{\theta=0}^{\pi} (E_{s\theta}H_{s\phi}^* - E_{s\phi}H_{s\theta}^*) r^2 sin\theta d\theta d\phi\right\} \tag{1.37}$$

which might be easily calculated thanks to (1.34) included into the expression of the scattered field and, after a bit of mathematical manipulations, we have:

$$W_s = \frac{\pi |E_0|^2}{k\omega\mu} \sum_{n=1}^{\infty} (2n+1) Re\left\{g_n\right\} \left(|a_n|^2 + |b_n|^2\right) \tag{1.38}$$

where $g_n = (\chi_n^*\psi_n^{'} - \psi_n^*\chi_n^{'}) - i(\chi_n^*\chi_n^{'} + \psi_n^*\psi_n^{'})$. This last definition can be simplified by the identity $\chi_n\psi_n^{'} - \psi_n\chi_n^{'} = 1$. Moreover this power could be *normalized*, that is to say, divided by the intensity from the incident light. Thereby, we introduce the associated cross section:

$$C_{sca} = \frac{W_s}{I_i} = \frac{2\pi}{k^2} \sum_{n=1}^{\infty} (2n+1)(|a_n|^2 + |b_n|^2) \tag{1.39}$$

In the same way, all of these previous step from (1.37) might be re-used for any other fields instead of the scattered field. Until now, only the light emitted by the particle was studied thanks to three fields: $(\mathbf{E}_i, \mathbf{H}_i)$, $(\mathbf{E}_s, \mathbf{H}_s)$ and $(\mathbf{E}_I, \mathbf{H}_I)$. However, it is possible to express a variable of extinction, opposed to the scattering *power* W_s, due to the interaction between the electromagnetic plane wave and our particle:

$$W_{ext} = W_s + W_a \tag{1.40}$$

This additional term, combined with the new one W_a, should be easily understood through a *power balance*, that is to say an energy balance replaced by the equivalent power. Indeed, if we denote W_a the amount of power which was varying during the interaction ($W_a > 0$ means that power is absorbed within the particle whereas $W_a > 0$ means that power is being created within the particle), it might be possible to write the following:

$$W_a = W_i - W_s + W_{ext} \tag{1.41}$$

As our actual medium is nonabsorbing, W_i vanishes identically and we retrieve the relation (1.40). Now, the extinction *power* might be evaluated in fonction of our previous vector spherical harmonic terms:

$$\begin{aligned} W_s = \frac{1}{2}\int_{\phi=0}^{2\pi}\int_{\theta=0}^{\pi} (&Re\{E_{i\phi}H_{s\theta}^* - E_{i\theta}H_{s\phi}^*\} + \\ &Re\{E_{s\phi}H_{i\theta}^*) - E_{s\theta}H_{i\phi}^*\}) \\ &r^2 sin\theta d\theta d\phi \end{aligned} \tag{1.42}$$

and, as stated above in (1.39), we finally obtain the extinction cross section by proportionality:

$$C_{ext} = \frac{W_{ext}}{I_i} = \frac{2\pi}{k^2} \sum_{n=1}^{\infty} (2n+1) Re\left\{a_n + b_n\right\} \tag{1.43}$$

At last, we have calculated and theoretically established the expression of two general terms which we might be retrieved by experiments: C_{sca} and C_{ext}. It is important to note that these cross section are, not only dependent on, but also strongly linked to our hypothesis, that is to say our input variables like the refractive index. Thereby, C_{sca} and C_{ext} are directly reliant on the size of our studied particle.

2 Simulations

2.1 Equations Adjustment

First at all, our main issue to numerically compute the cross sections C_{sca} and C_{ext} is to calculate the associated scattering coefficients a_n and b_n. Globally, these two numbers are obtained through Bessel functions as we can see from (1.34) and our goal is to retrieve each value of them between a certain range of wavelength in order to obtain a kind of spectrum. However, due to the size of our nanoparticle close to the incident wavelength included in a visible range, the variable $\rho = kr$, as a dependency for the Bessel functions, is also restrained into a small range of value close to zero along the x-axis. In fact, in the context of a computer, these targeted values could be too sensitive to be calculated with a reasonably high precision. Thereby, we could introduce the *logarithmic derivative*:

$$D_n(\rho) = \frac{d}{d\rho} ln[\psi_n(\rho)] \tag{2.1}$$

Thanks to this additional definition, we are expanding the range of hit values and decreasing the sensitivity. In this way, we can rearrange the expressions of a_n and b_n from (1.34):

$$\begin{aligned} a_n &= \frac{[D_n(mx)/m + n/x]\psi_n(x) - \psi_{n-1}(x)}{[D_n(mx)/m + n/x]\xi_n(x) - \xi_{n-1}(x)} \\ b_n &= \frac{[mD_n(mx) + n/x]\psi_n(x) - \psi_{n-1}(x)}{[mD_n(mx) + n/x]\xi_n(x) - \xi_{n-1}(x)} \end{aligned} \tag{2.2}$$

where we have used the recurrence relation:

$$z_n^{'}(x) = z_{n-1}(x) - \frac{n z_n(x)}{x} \tag{2.3}$$

with z_n replaced by ψ_n or ξ_n. Note that x is not a constant because of its dependency through λ that we are going to slide along our targeted range. Moreover, due to the recurrence relations of Bessel functions explained below, in the next subsection, D_n also satisfies the following relation:

$$D_{n-1}(\rho) = \frac{n}{\rho} - \frac{1}{D_n(\rho) + n/\rho} \tag{2.4}$$

Because of the link existing between D_n and Bessel functions, this previous recurrence (2.4) should be runned downwardly, that is to say begining with the higher n owned by the scattering coefficients, in order to avoid the unstability of our computation as stated in the subsection below. Otherwise, the calculated data could be rapidly *flawed* while n is increasing.

2.2 Computation of Bessel Functions

Then, our last issue is to numerically compute the spherical Bessel functions, as the first, second and the associated Hankel functions or even the Ricatti-Bessel functions. Hopefully, in our preferred scientific language that is *Python*, all of these features are already implemented. Thereby, as a first approach and taking into account that *Mie Theory* is not really heavy, it is completly useless and counterproductive to re-write this mathematic area. However, it could be interesting to speed up the computation thanks to a low-level programming language, or more generally, a compiled one. At least, for a better understanding of the computation, we can define a way to numerically implement these tools.

To contextually replace our problem, these Bessel functions are introduced in our theory through the resolution of the radial part (1.15) in order to get a global expression of the generating couple of function ψ_{emn} and ψ_{omn}. Involving spherical coordinates in our calculation, we must use the spherical Bessel functions j_n and y_n which are a special case of general Bessel functions J_n and Y_n solving the Bessel's differential equation:

$$x^2 \frac{d^2y}{dx^2} + x\frac{dy}{dx} + (x^2 - \alpha^2)y = 0 \tag{2.5}$$

where α is a complex number without restriction. Thereby, we have the following definitions:

$$j_n(x) = \sqrt{\frac{\pi}{2x}} J_{n+\frac{1}{2}}(x) \qquad y_n(x) = \sqrt{\frac{\pi}{2x}} Y_{n+\frac{1}{2}}(x) \tag{2.6}$$

Note that the actual x might be real or a complex value and is, by definition, different from all previous sections.

After some mathematics calculation, it is possible to demonstrate the following recurrence relations:

$$\frac{2n+1}{x} z_n(x) = z_{n-1}(x) + z_{n+1}(x) \tag{2.7}$$

$$(2n+1)\frac{d}{dx} z_n(x) = n z_{n-1}(x) - (n+1) z_{n+1}(x) \tag{2.8}$$

where z_n is either j_n or y_n. Thanks to these previous equations (2.7), and given the two first exact expression for the spherical Bessel functions, we can theoretically obtain all wished order n. So, *by hand*, we have the following:

$$\begin{aligned} j_0(x) &= \frac{sin(x)}{x} \qquad & j_1(x) &= \frac{sin(x)}{x^2} - \frac{cos(x)}{x} \\ y_0(x) &= -\frac{cos(x)}{x} \qquad & y_1(x) &= -\frac{cos(x)}{x^2} - \frac{sin(x)}{x} \end{aligned} \tag{2.9}$$

with the associated figures:

Thereby, by inverting the main recurrence relations (2.7) into this way:

$$z_{n+1}(x) = \frac{2n+1}{x} z_n(x) - z_{n-1}(x) \tag{2.10}$$

we should be able to compute the next order $n = 2$ for a given x either real or complex. Continuing with the same idea, we can obtain j_3, j_4... coupled with the associated

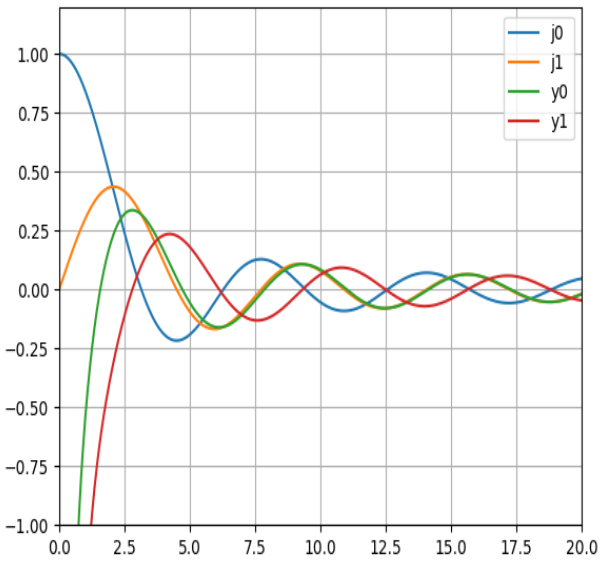

Figure 2: j_0, j_1 with y_0, y_1

y_n. This way to compute all wished spherical Bessel function, or more generally any function recursively defined, from the lowest order $n = 0$ reaching the highest order $n = \infty$, is commonly called an *upward recurrence*. Assuming that we have in our possession a couple of spherical Bessel function at the order $n = i$ and $n = i + 1$, an opposed computation from the previous one, should allow us to recursively reach $n = 0$:

$$z_{n-1}(x) = \frac{2n+1}{x} z_n(x) - z_{n+1}(x) \tag{2.11}$$

that is called a *downward recurrence* because of the decrement of n for each calculated value. Despite these two recursive ways are strictly equivalent from a mathematical point of view, there is a not negligible difference between them. Indeed, taking into account boundaries of coding number (currently 64 bit for a common *float*) and the behavior of spherical bessel functions, it is possible, but tough, to demonstrate either the stability or the unstability for the first and second kind calculated through downward or upward reccurency. Otherwise, by a *hand* way, we can easily retrieve these theoritical results by comparing our calculations with exact curves already tabulated:

- Stable by **upward** recurrency:
  - $y_n, \forall x$
  - j_n, if $|x| \geqslant n$
- Stable by **downward** reccurency:
  - j_n, if $|x| < n$

assuming that $Re\{x\} \in \mathbb{R}_+$. Now, we can think about the programming steps in order to compute our spherical Bessel functions of the first and second kind through an upward recurrency: we get j_0/y_0 and j_1/y_1 from a given x then, thanks to (2.10), we compute all required order j_n/y_n with $n \geqslant 2$. However, a question remains in a downward reccurency: How to get starting Bessel function values for higher order $n = i$ and $n = i + 1$?

Theoretically, it is well know that Bessel functions of the first kind J_n satistfies the following relation:

$$\forall\, x \,|\, Re\{x\} \in \mathbb{R}_+, \lim_{n\to\infty} J_n(x) = 0 \tag{2.12}$$

Thereby a common approach, called the *Miller* method, is to suppose that our targeted higher order i is arbitrary equal to 1 whereas the $i + 1$ order is null. Afterward, we can easily pull down the order thanks to (2.11). Once we obtain the first order $n = 0$, because of the linearity of our recurrence relations, we *normalize* this serie by the true value of $j_0(x)$.

For example:

$$\begin{aligned} j_{i+1}^{computed}(x) &= 0 \\ j_i^{computed}(x) &= 1 \\ j_{i-1}^{computed}(x) &= \frac{2i+1}{x} j_i^{computed}(x) - j_{i+1}^{computed} \\ &\dots \\ j_0^{computed}(x) &= \alpha \end{aligned} \tag{2.13}$$

Now, we can *normalize*:

$$\begin{aligned} j_0(x) &= \frac{sin(x)}{x} \qquad \text{(by definition)} \\ j_0^{final}(x) &= j_0^{computed}(x) \times \frac{j_0(x)}{\alpha} = j_0(x) \\ j_1^{final}(x) &= j_1^{computed}(x) \times \frac{j_0(x)}{\alpha} \\ &\dots \\ j_i^{final}(x) &= j_i^{computed}(x) \times \frac{j_0(x)}{\alpha} \end{aligned} \tag{2.14}$$

where j_X^{final} is the wished result. In fact, we just have *normalized* our serie $j_X^{computed}$ by the initial factor $\frac{j_0(x)}{\alpha}$. It is important to notice that any serie constructed through this way always verifies the recurrence relation (2.10) and each term is, by definition, a solution of the radial part (1.15).

Unfortunately, a last issue still remain in our downward recurrency approach. Something that is not obvious at the first glance, we see that for a given i and for any x, the serie $j_X^{computed}$ always has the same value for all terms in it. That is to say, only the *normalization* factor introduce the value x in our final serie and, finally, $j_X^{computed}(x)$ is not really dependent on x (we can omit this parameter afterwards). In this way, due to the mathematical shape of our recurrence relation (2.11), each value of a lower computed order is bigger than its previous higher order: $j_0^{computed} > j_1^{computed} > ... > j_i^{computed}$. So, if we target a really high order with, for instance, $i = 10^{10}$, the first order will ineluctably get a really high value. Thereby, for a computer with *physical* boundaries for its numbers, this previous result will give us an invalid value for an intermediate order and all order below will be saturated with the

same invalid state. In this way, the *normalization* step is impossible because α in (2.14) will own a *NaN* value (that is a computer overflow indicator). Even if, for a first approximation, we use the ten first order for calculation, this phenomenon will be rapidly visible even for our range of value (from $n = 50$) and it could be intersting to avoid this *blocking* state. So, the first solution proposed in many other articles treating the *Mie Theorie*, or more generally the computation of Bessel functions, is to set an arbitray minimal value for i, that is to say 10^{-10} instead of 1. However, this method will only postpone the phenomenon. A second solution is to divide the downward reccurency into multiple chunks. As mentioned above, $j_X^{computed}$ is recursive and completly dependent on the targeted order i. In fact, if we want $i = 1000$ as a final order, we can calculate $j_X^{computed}$ from $n = 0$ to $n = 50$ (stability limit) and apply a normalization as previously stated for this first chunk. Secondly, we compute a second chunk starting from $n = 50$ to $n = 100$ (actually, the computation begins with $n = 100$ because of the downward behavior). Then, it is possible to assume that $\{j_0^{computed} \cdots j_{50}^{computed}\} = \{j_{50}^{computed} \cdots j_{100}^{computed}\}$ due to the arbitrary recurrence relation. For the second chunk, we can normalize it by $j_{50}^{computed}$ from the first chunk, itself normalized by the exact $j_0(x)$ (which is not arbitrary but dependent on x). This method is chain-shaped and we recursively advance, chunk by chunk to finally obtain every order wished without overflowing the computer results.

2.3 Input Variables

At this point of our simulation part, we have to precisely fix and set our input variables, that is to say with, roughly, this following pattern:

$$Output = Simulation(Input) \tag{2.15}$$

where *Output* is our wished scattering and extinction cross sections. Given the relations (1.39) and (1.43) coupled with the expressions of a_n and b_n previously established, we are able to recognize these variables. Thereby, all inputs are included into (1.32) with refractive indices of the medium N_I and the particle N, the particle's size a then the wavelength λ.

First at all, let's consider the λ variable. The problem is the following: from our theory, we send an incident monochromatic light, that is to say $\lambda = constant$ in the visible range. However, in reality, the experimental tool produce multiple monochromatic lights in order to reach all values in the visible range and compute the associated cross sections. In fact, the wavelength λ will vary for each computation and, by the way, is an *Input* variable. Therefore, we have $x = x(\lambda)$ and more precisely $k = k(\lambda)$

Secondly, the particle's size a represents the radius of this last one. Obviously, from the purpose of this study, it is also an *Input* variable.

Then, the refractive index of the medium, taking into account that the environment is homogenous, this last one is a constant value. Even more, if we consider that the medium is the ambiant air, it might be possible to approximate it as the void and finally set $N_I = 1$. Moreover, we have now the following relation $m = N$.

The last variable to describe is the refractive index N of our particle. At this point, we can introduce the targeted material, that is to say, the substance used into our spherical sample: silicon. As a first approximation, we can say that silicon has a constant refractive index commonly setted around 3.5. Thereby, for $a = 100^{-9}m$ and $\lambda = [206^{-9}, 826^{-9}]$ (visible range a bit extended in the *UV* range), we obtain the following cross sections: where *Sca*

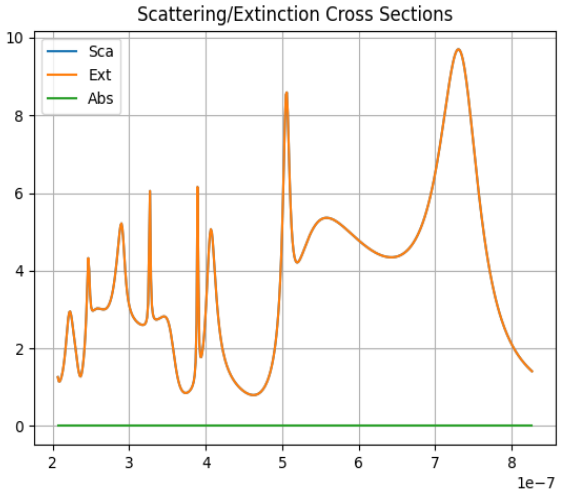

Figure 3: Cross sections with $N = 3.5$

is the scattering, *Ext* the extinction and *Abs* the absorbtion cross section linked with (1.40): $C_{abs} = C_{ext} - C_{sca}$. We can see that there is no absorbtion and the scattering cross section equals the extinction one. However, to properly describe physical states of matter, we have to consider that the refractive index is varying depending on the wavelength of the incident light, that is to say, $N = N(\lambda)$. In this way we obtain: where we use the real

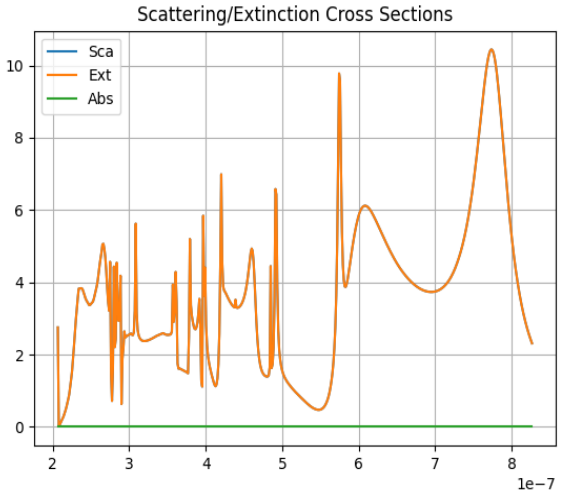

Figure 4: Cross sections with $N = N(\lambda)$

part of pre-computed refractive indices from another scientific experiment (Aspnes and Studna, 1983). We easily see that the main maximums, called *Mie resonances*, are shifted to the right but this approach globally keep the previous shape. It is always remarkable that $C_{sca} = C_{ext}$. That is due to the real expression of the refractive index. Indeed, the absorbtion behavior of our material is mathematicaly implemented through the imaginary part of N. In this way, we should have $N = N_{re} + iN_{im}$ Thereby, when we use a complex varying index, we obtain: Now,

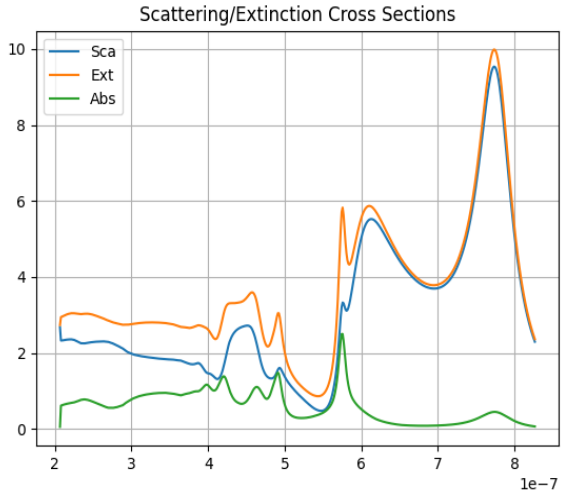

Figure 5: Cross sections with $N = N(\lambda)$ complex

in addition to the previous shape then according to each Mie's resonance pike, we have a maximum of absorbtion describing the capacity of our particle to redistribute the energy of the incident light into another form, like a thermal energy. It is important to notice that the varying imaginary part doesn't change the position of the pikes in contrary to the varying real part.

Finally, our *Input* variables are the following: a (particle's size), λ (incident light's wavelength) and $N(\lambda)$ (refractive index depending on λ).

2.4 Results

Finally, we are able to compute our required *Output* which are the scattering C_{sca} and extinction C_{ext} cross sections. As a reminder and as stated in the end of the *theory* part, these last are relevant in the study of nanoparticles because cross sections are directly linked to the size of the particle.

First at all, it could be interesting to visualize the different contributions of each terms in cross section expressions (1.39) and (1.43). Indeed, these two relations are primarly composed of an infinite sum which might be *separated* in order to compute the associated a_n and b_n terms roughly as following:

$$\sum_{n=1}^{\infty} f_n(a_n) + f_n(b_n) = \sum_{n=1}^{\infty} f_n(a_n) + \sum_{n=1}^{\infty} f_n(b_n) \quad (2.16)$$

where $f_n(X) = \frac{2\pi}{k^2}(2n+1)Re\{X\}$ in the case of C_{ext} (with a similar expression for C_{sca}). In this way, for an arbitray particle defined by a radius of $100e^{-9}$ meters, we obtain (6) then (7) for the scattering and extinction cross section respectively. These figures show that each

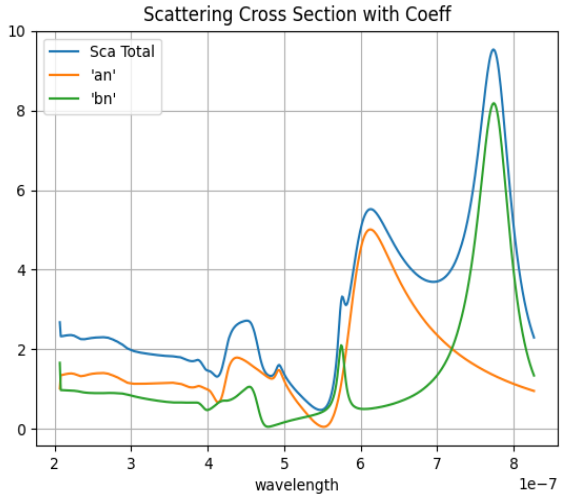

Figure 6: C_{sca} coefficient contributions

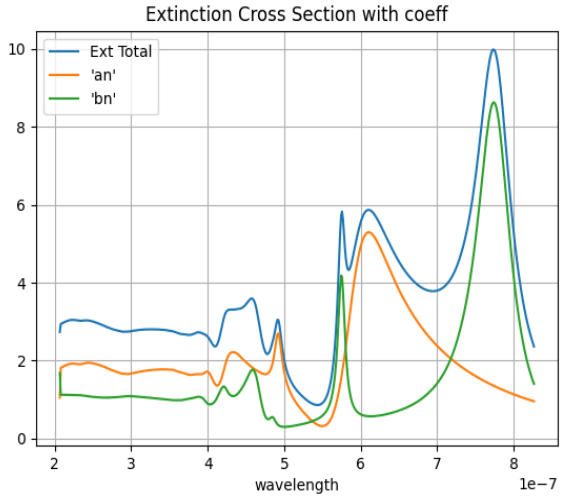

Figure 7: C_{ext} coefficient contributions

local maximum is due to a heavy weighting from one or the other of the coefficients. More particularly, the global maximum called *principal Mie's resonancy* seems to be be generated by the second coefficient b_n whereas the first one, a_n influences the second global maximum which is located on the left of the first maximum.

Secondly, as stated in the previous subsection, we have three *Input* variables that we can potentially change. Note that the incident light's wavelength is fixed by the targeted range of value for the *extended*-visible light and the refractive index of our particle, depending on λ, is, him too, fixed by the material studied: silicon. Thereby, our last *free* parameter is the size or more precisely the radius. Therefore, when varying this *Input* variable, we

obtain (8) and (9) associated to C_{sca} and C_{ext} for three different sizes surrounding all possible particles encountered during the experiments. As we can see, it is possible to consider a *recursive* shape which is composed by the boundary of the first and second global maximum. In fact, the principal Mie's resonancy is moving left when the size decreases and reciprocally. Moreover the scale and the maximum y-value are also decreasing. However, it might be roughly possible to assess that, for our targeted range of values, this shape thus defined is moving left for smaller sizes then right for larger sizes.

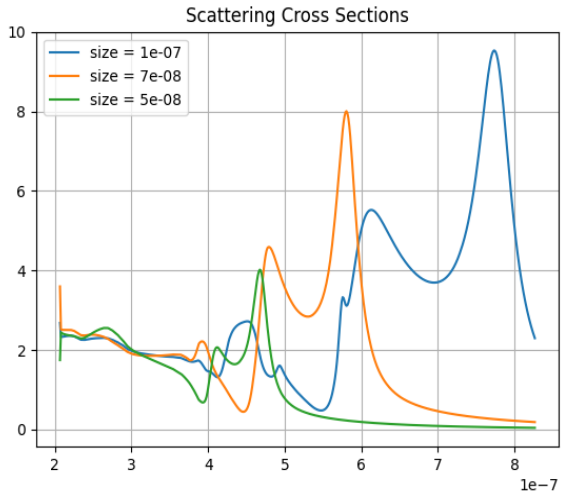

Figure 8: C_{sca} for three different sizes

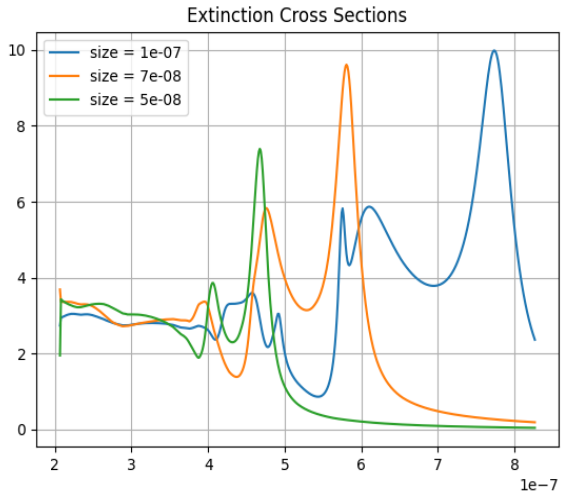

Figure 9: C_{ext} for three different sizes

After all, if we reproduce our computations with, this time, the radius as a *real* free parameter instead of an arbitrary fixed value, we obtain the following figures (10) and (11) for the scattering and extinction cross sections respectively. In this way, we can easily visualize our wished *Output* results and compare later with the collected experimental data. Now, it is obvious that, as a really first approximation in our range of values, each maximum and, more particularly, the two global maximum represented by the most intense yellow lines, could be calculated through a linear equation with a different coefficient each explaining, by the way, the compression of the defined shape for smaller radius. **Retrieve the linear equation for the principal Mie's resonancy and compare**

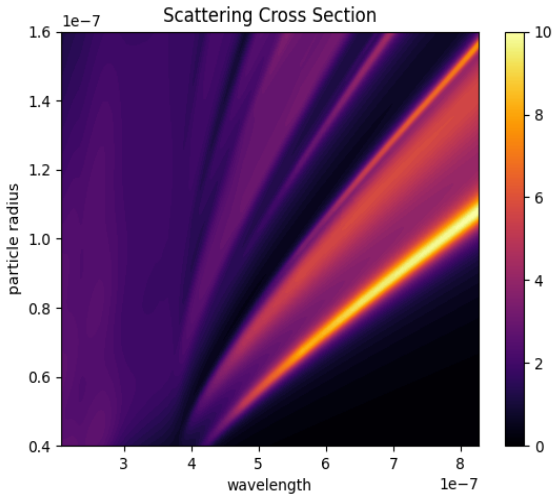

Figure 10: C_{sca} depending on radius and wavelength

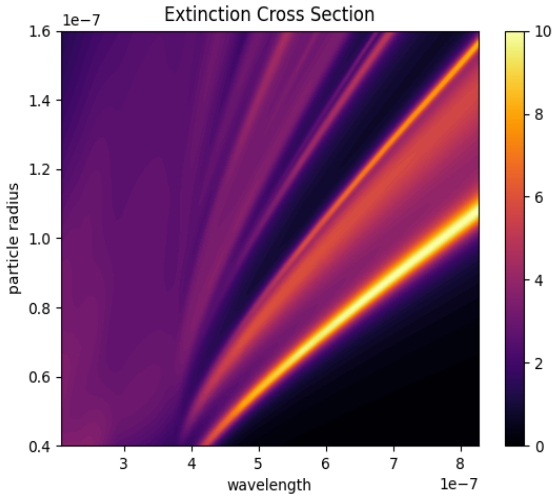

Figure 11: C_{ext} depending on radius and wavelength

3 Experiments

3.1 Base Description

First, let's describe the procedure to experimentaly test and compare our simulation part. In theory, our studied particle should have a spherical shape and, as stated in the previous section, the associated material should be *silicon*. Thereby, we are supposed to create a sample composed of spherical nanoparticles of silicon with different sizes included between $100nm$ and $200nm$

of diameter. Moreover, in order to approve our theorical approach and all of the approximation employed until now, we have to retrieve experimentaly the *defined shape* made up of the first and second principal Mie resonancies linked with an equivalent gradient. In fact, our different sized nanoparticles being randomly scattered on the sample, we have to collect the size of some nanoparticles coupled with both scattering and extinction cross section spectrums. In this way, we will be able to link C_{sca} and C_{ext} shapes according to the respective sizes to finally check if those actually fit the simulation. Therefore, the tools used to collect each spectrums associated with the size are the *optical* and *atomic force* microscopes respectively.

3.2 Sample Preparation

Chronologically, the first experimental stuff we have to realize is the preparation of the silicon nanoparticle sample.

First of all, we have to find a proper support for our different particles. In this way, we use a glass substrat which is composed of a matrix where micrometric number elements are engraved on the bottom side, in order to see and locate the position of our experiment area on this sample during observation through optical or AFM microscopes. The substrat has the particularity to be transparent which allow the light to cross it and let numbers to be visible as shown on figure (12). Moreover,

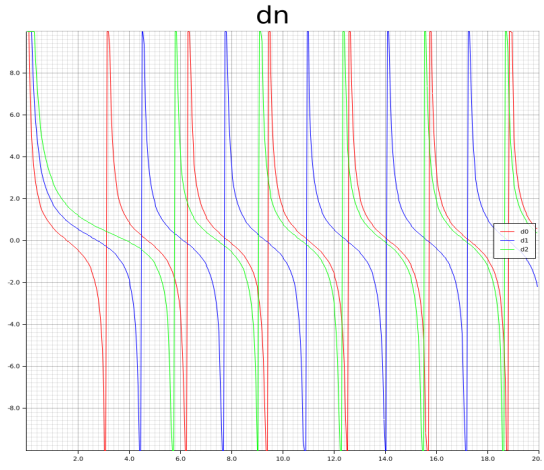

Figure 12: glass substrat

our goal being to put nanoparticles on this substrat, we have the following layers described on figure (13). From a technical point of view, the base glass substrat is too large to be placed on the different microscope. Thereby, this last one must be broke into several pieces, each with dimensions smaller than $2 \times 2cm$.

Secondly, we have to physically produce silicon nanoparticles with *random* sizes included between $50nm$ and $100nm$ in radius. Hopefully, this step is realized thanks to another research team from the *DTU* (see ...). Globally, they are created from SiO lumps annealed at, approximately, $1500C$ then etched to produce Si nanoparticles in a solution.

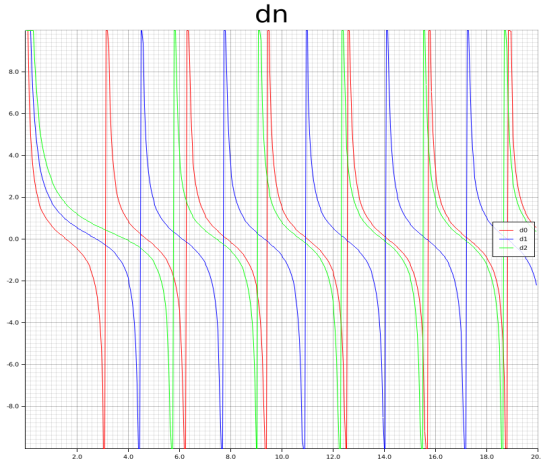

Figure 13: substrat layers

Finally, these nanoparticles are placed on the glass substrat pieces thanks to a micropipette: we put a droplet of around 10 microliter on each chip. Afterward, we must either dry in air, or blow dry to progressively remove water from the samples. In the end, our silicon nanoparticles are *dropcasted*.

3.3 Optical Microscope

3.4 Atomic Force Microscope

At this point of the experiment part, we have to couple the spectrum, previously retrieved thanks to the optical microscope, with the size of each studied particle. Thereby, we need another kind of tool in order to detect physically the wished size, that is to say, an instrument able to mesure the diameter, or at least to give an equivalent data, of the desired particle instead of collecting the scattered light intensity. In this way, the best suited tool for this task is the *atomic force microscope*.

The working principle of that kind of microscope is pretty simple. At our *human* scale, the operating mode is roughly similar to the Braille system. Indeed, our sample being totally flat at a macroscopic point of view, the main idea is to drag a tip on the desired experimental surface. This tip is directly connected to a detector collecting the nanometric height variations along the advancement of the last one as shown on figure (14). In this way, if the tip runs into a nanoparticle, it could be possible to substract the maximum height to the base one, referencing the surface's sample which is the minimum in that case, in order to get the diameter of the particle (assuming that those are spherical).

Technically, even if in general an AFM can use different methods to scan the sample, in our case, the microscope use the *Van der Waals* forces existing between the tip and the nanoparticles. These forces are responsible of the attraction between atoms in a molecule, for instance. Thereby, with no movement, the tip is in balance above the sample without touching it: this is a *non-destructive* scanning tool. The height detector itself is composed of a laser reflecting on the end piece of the cantilever main-

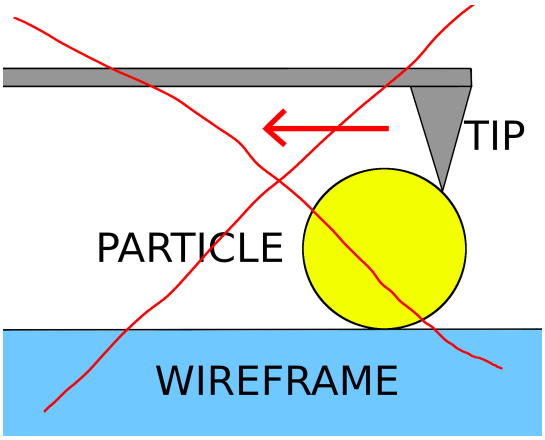

Figure 14: AFM working principle

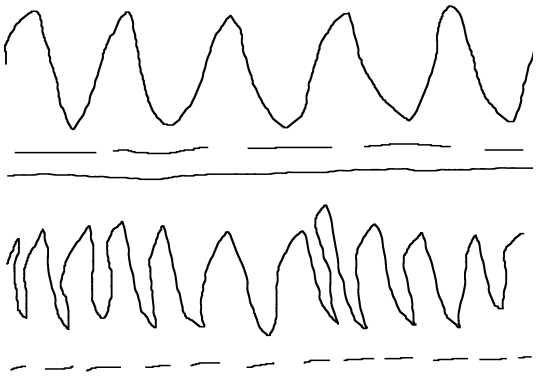

Figure 16: AFM point configuration

taining the tip. When we scan a sample, the tip attached to the cantilever and the laser are moving as a whole block and the tip oscillate around its balance position. In this way, if the tip moves up, compared to its small oscillations, because of a nanoparticle (or another kind of *perturbartion*), the optical way runned by the light, and emited from the laser, is shorter: we detect a height variation. Effectively, the same process happens when the tip moves down. Then, in order to scan a sample, the tip must move along an arbitrary line and, with a pre-defined length, must shift on the next line to reproduce this task until the quantity of line correspond to the length of these last. Afterward, we obtain a square shaped area of our sample. Moreover, as shown on figure (15), multiple scanning modes are available like a double sens scan, that is to say, the tip re-run the scanned line instead of moving out it at the end point, or an horizontal/vertical direction scan, that is to say, the scanned line might be oriented North-South or East-West, and even a start/end point selector, among plenty of other configurations. Additionaly,

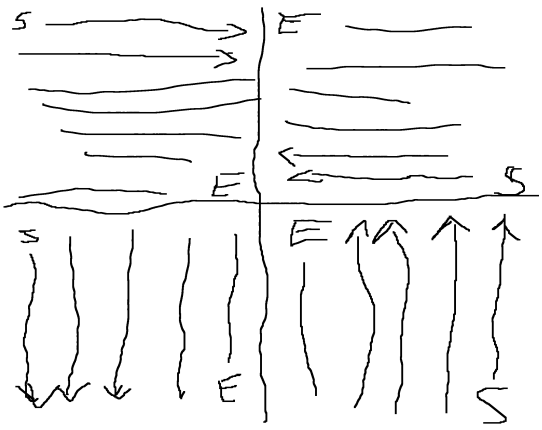

Figure 15: AFM direction configuration

as the tip is slightly oscillating around its balance position, it is possible to choose the amount of scanned *points* as shown on figure (16), that is to say, the number of periods made compared to the advancement of the system (tip, cantilever and laser) corresponding to the amount of generating pixels for a line. This parameter, associated with the user-defined line's length, might increase or decrease the quality of the collected data. However, increasing the image resolution increases the scanning time by the same. As a rough idea, to scan a $200 \times 200nm$ square with 100 points/pixels takes around 10 minutes whereas, for a $50 \times 50nm$ area with 256 points/pixels takes the same amount of time. Therefore, a precise distribution must be adopted between quality, surface and speed in order to collect enough data and retrieve the nanoparticle's size.

In order to illustrate the whole procedure to retrieve the associated size of our studied particle, we will arbitrary choose a nanosphere of silicon as shown on figure (17). At first glance, knowing that a blue scattered light

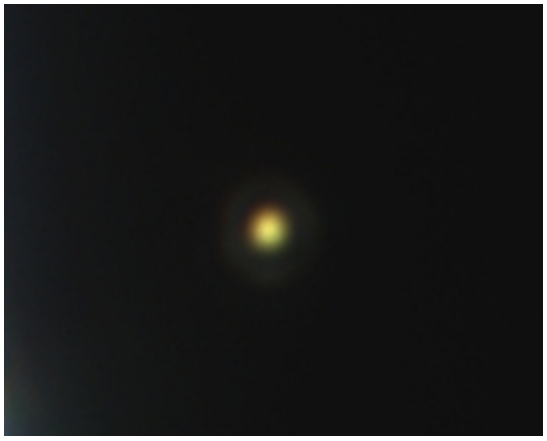

Figure 17: Example Particle's Image (Dark Field)

is equivalent to the *smallest* size ($\sim 50nm$) whereas a red color means the *biggest* one ($\sim 100nm$), we can easily say that through the yellow-orange color emitted by this particle, we approximate $80nm$ of radius. However, we need more precision to check our simulation. Thereby, we use the AFM microscope and execute a scan of the targeted area. Unfortunately, for some technical reasons, collecting the final data with enough *quality/pixels* to analyse, requires multiple scan in *low quality* and *large dimension* to locate the right particle. Finally, we obtain the following image (18), through the *Gwyddion* software specialized in AFM data analysis, with a resolution of 256

pixels/points for the line's width. Note that the scan pro-

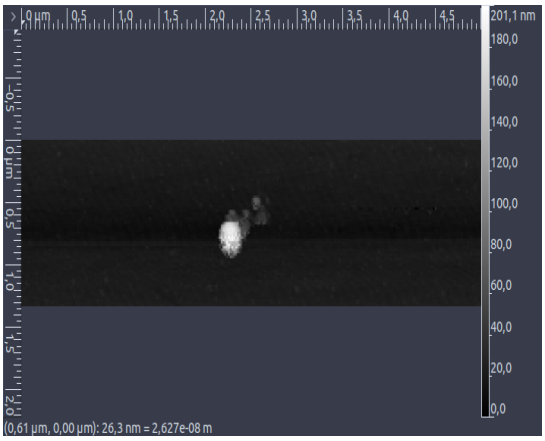

Figure 18: Example Particle's Scan

cedure, started from the bottom side, was aborted when the particle has entirely been scanned: that is why we observe a rectangular area instead of a squared one. Now, it is much more easier to visualize and get the proper data. As we can see, the shape of our particle is close to a disc although some residual silicon *waste* on the North-East side. However this image don't reveal the exact diameter, even if we assume a spherical particle, because of the random pertubration on the edge due to the oscillations of the tip when encountering a particle. In this way, the height, being graduated thanks to a grey-scale put on the right, will give us the maximum of the scan. It is already possible to approximate the diameter as included between $160nm$ and $190nm$. Then, we use a tool from the software, exctracting precisely the height scanned along a specific line as shown on figure (19). The exctracted

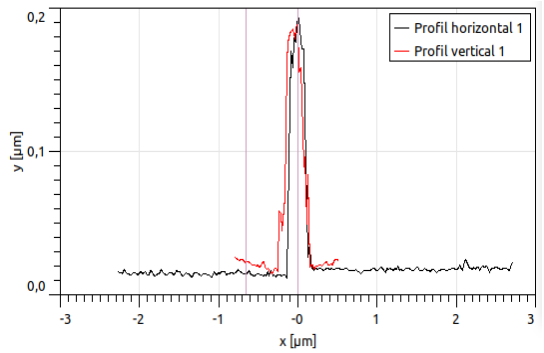

Points	X [µm]	Y [nm]	Longueur [µm]	Hauteur [nm]	Angle [deg]
	-0,000	191,5			
	-0,655	14,7	-0,655	-176,7	-164,91

Figure 19: Example Particle's Measurements

pattern was put on the arbitrary defined top of the particle, that is to say the most white part, producing an horizontal and vertical line in black and red respectively. Therefore, we can differentiate the height between the *flat* area and the maximum in order to retrieve the diameter which is, in this case, $176.7nm$ giving approximately $88nm$ and confirm our first hypothesis.

4 Discussion